

## Hydrothermal Synthesis of Terbium doped Antimony Selenide Nanomaterials and Investigation of Their Photocatalytic Performance

Younes Hanifehpour <sup>✉1</sup>  | Negin Rahmani <sup>2</sup>  | Sang Woo Joo <sup>✉3</sup> 

1. Correspond author, Department of Chemistry, Sayyed Jamaledin Asadabadi University, Asadabad, Iran. E-Mail: younes.hanifehpour@gmail.com
2. Department of Chemistry, Sayyed Jamaledin Asadabadi University, Asadabad, Iran. E-Mail: rahmani.negin2004@gmail.com
3. Correspond author, School of Mechanical Engineering, Yeungnam University, Gyeongsan 712-749, Korea. E-Mail: swjoo1@gmail.com

### Article Info

**Article type:**  
Research Article

**Article history:**

Received 6 July 2023

Received in revised form 16 August 2023

Accepted 1 September 2023

Published online 9 October 2023

**Keywords:**

Terbium,  
Rhodamine B,  
Hydrothermal,  
Semiconductor,  
Photocatalyst.

### ABSTRACT

Tb<sup>3+</sup>-doped antimony selenide nanomaterials were prepared via a hydrothermal route through the co-reduction method. The obtained products were characterized utilizing Scanning electron microscopy (SEM), X-ray photoelectron spectroscopy (XPS), transmission electron microscopy (TEM) and X-ray powder diffraction (XRPD). Powder XRD patterns indicate that the Tb<sub>x</sub>Sb<sub>2-x</sub>Se<sub>3</sub> crystals (x = 0.00-0.1) are isostructural with Sb<sub>2</sub>Se<sub>3</sub>. SEM images show that doping of Tb<sup>3+</sup> ions in the lattice of Sb<sub>2</sub>Se<sub>3</sub> results in nanoparticles. The electrical conductance of terbium-doped antimony selenide is higher than undoped Sb<sub>2</sub>Se<sub>3</sub> and increases with temperature. The synthesized nanomaterials were used as heterogeneous photocatalysts for the degradation of some water pollutant organic dyes under direct visible (with fluorescent light with 40 W Power). Rhodamine B (RB) was used as a typical dye to obtain the optimum photocatalytic degradation conditions. The photocatalytic reaction yield was 76% at the present conditions. The influence of radical scavengers on degradation percentage was investigated.

**Cite this article:** Hanifehpour, Y. Rahmani, N. & Woo Joo, S. (2023). Hydrothermal Synthesis of Terbium doped Antimony Selenide Nanomaterials and Investigation of Their Photocatalytic Performance, *Advances in Energy and Materials Research*, 1 (1), 23-28. <https://doi.org/10.22091/JAEM.2023.9656.1005>



© The Author(s).

DOI: <https://doi.org/10.22091/JAEM.2023.9656.1005>

Publisher: University of Qom.

## 1. Introduction

The degradation of hazardous organic pollutants existing in industrial wastewater via advanced oxidation processes (AOPs) has been an active area of research. The fundamental mechanism of AOP is the production of  $\bullet\text{OH}$  radical with high oxidization potential to achieve faster and more efficient degradation of the contaminants. The AOP procedure is particularly effective for cleaning biologically toxic or non-degradable materials such as pesticides, aromatics, petroleum constituents, and volatile organic compounds in wastewater [1–4].

Rare earth ions doped inorganic nanomaterials with various compositions have become an increasingly important research topic and opened up the opportunity for creating new applications in diverse areas, such as light-emitting displays, biological labeling, and imaging [5–7]. Investigations on semiconductor nanostructures have recently been the focus of intensive research activities because of intrinsic fundamental interest and manifold possibilities for applications. Semiconductor selenides find applications as laser materials, optical filters, sensors, and solar cells. Antimony selenide, an important member of these  $\text{V}_2\text{VI}_3$  compounds, is a layer-structured semiconductor of orthorhombic crystal structure and exhibits good photovoltaic properties and high thermoelectric power (TEP) which allows possible applications for optical and thermoelectric cooling devices [8–10]. Studies of impurity effects or doping agents on the physical properties of  $\text{Sb}_2\text{Se}_3$  are interesting both for basic and applied research. Doping of trivalent cations such as  $\text{Mn}^{3+}$  [11],  $\text{Fe}^{3+}$  [12],  $\text{In}^{3+}$  [13],  $\text{Sb}^{3+}$  [14], and several further trivalent 3d elements [15] to the lattice of  $\text{Bi}_2\text{Se}_3$  have been investigated, also EPR spectra of Gd-doped bulk  $\text{Bi}_2\text{Se}_3$  [16]. However, there is no report about the doping of terbium into the lattice of  $\text{Sb}_2\text{Se}_3$ . The incorporation of large electropositive ions such as lanthanides into antimony chalcogenide frameworks is expected to lead to materials with various properties. The incorporation of lanthanide ions into an Sb–Se framework could dramatically affect the electronic properties of that framework.

## 2.1. Materials and methods

All of the utilized chemicals were of explanatory grade, gotten from commercial sources, and utilized without encouraging decontamination. Stage distinguishing pieces of proof were performed on a powder X-ray diffractometer D5000 (Siemens AG, Munich, Germany) utilizing  $\text{CuK}\alpha$  illumination. The morphologies of the gotten materials were inspected with a field emanation checking electron magnifying lens (Hitachi FE-SEM demonstrate S-4160).

Absorption spectra were recorded on an Analytik Jena Specord 40 (Analytik Jena AG Explanatory Instrumented, Jena, Germany). The surface zone and pore volume and normal nanoparticles estimate were calculated utilizing the Brunauer-Emmett-Teller (Wagered) condition. Pore measure conveyances, pore volume, and pore surface region were calculated by the Barrett-Joyner-Halenda (BJH) strategy.

## 2.2. Fabrication of catalyst

All chemicals were of analytical grade and used without further purification. Grey selenium (0.237 g, 1 mmol) and NaOH (0.7 g) were added to distilled water (50 mL) and stirred well for 15 min at room temperature. Afterward,  $\text{SbCl}_3$ , hydrazinium hydroxide (2 mL, 40 mmol), and  $\text{Tb}(\text{NO}_3)_3 \cdot 6\text{H}_2\text{O}$  with stoichiometric ratios were added, and the mixture was transferred to a 100 mL Teflon-lined autoclave. The autoclave was sealed, maintained at 160 °C for 24 h, and then cooled to room temperature. The black precipitate obtained was filtered and washed with ethanol and water. It was then dried at room temperature. Yields for the products were 81–85 %.

## 3. Results and Discussion

$\text{Sb}_{2-x}\text{Tb}_x\text{Se}_3$  samples were prepared by a hydrothermal co-reduction method. The powder X-ray diffraction patterns (see Figure 1) indicate that the  $\text{Tb}^{3+}$ -doped powders have the same orthorhombic structure as  $\text{Sb}_2\text{Se}_3$  and that single-phase  $\text{Sb}_2\text{Se}_3$  is retained at lower doping concentrations of  $\text{Tb}^{3+}$ . All the peaks in Figure 1 can be attributed to the orthorhombic phase of  $\text{Sb}_2\text{Se}_3$  with lattice parameters  $a=11.62 \text{ \AA}$ ,  $b=11.76 \text{ \AA}$ , and  $c=3.95 \text{ \AA}$  (JCPDS card File:72-1184). Beyond doping levels of  $x = 0.10$  for  $\text{Tb}^{3+}$  additional unknown phases were seen.

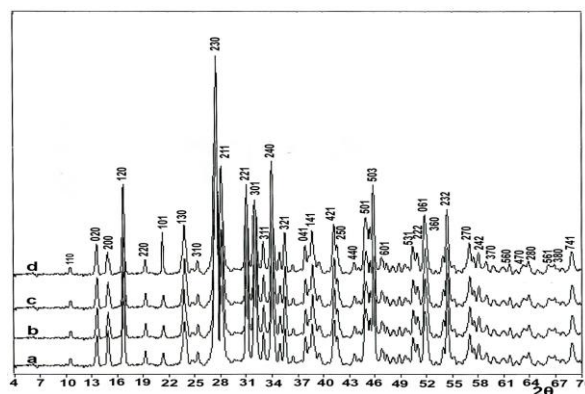


Figure 16. Powder X-ray diffraction pattern of  $\text{Sb}_{2-x}\text{Tb}_x\text{Se}_3$  (a:  $x = 0.0$ , b:  $x = 0.04$ , c:  $x = 0.08$ , d:  $x = 0.1$ ) synthesized at 160°C and 24h.

The EDX analysis of the product confirms the ratio of Sb/Se/Tb as expected (see Figure 2). Also, ICP analysis confirms the exact amount of doping.

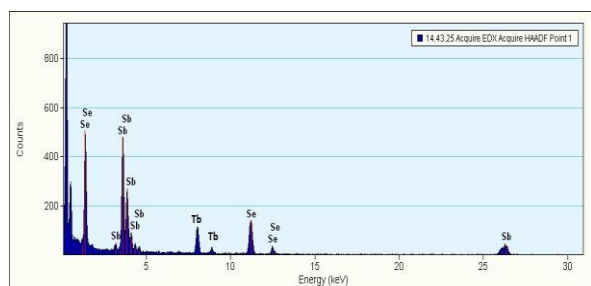


Figure 17. EDX patterns of  $Sb_{2-x}Tb_xSe_3$  synthesized at  $160^\circ C$  and 24h.

The cell parameters of the synthesized materials were calculated from the XRD patterns. With increasing dopant content ( $x$ ), the  $a$ ,  $b$ , and  $c$  parameters for  $Tb^{3+}$  increase, as shown in Figure 3. The trend for lattice constants can be correlated to the effective ionic radii of the  $Tb^{3+}$  ions.

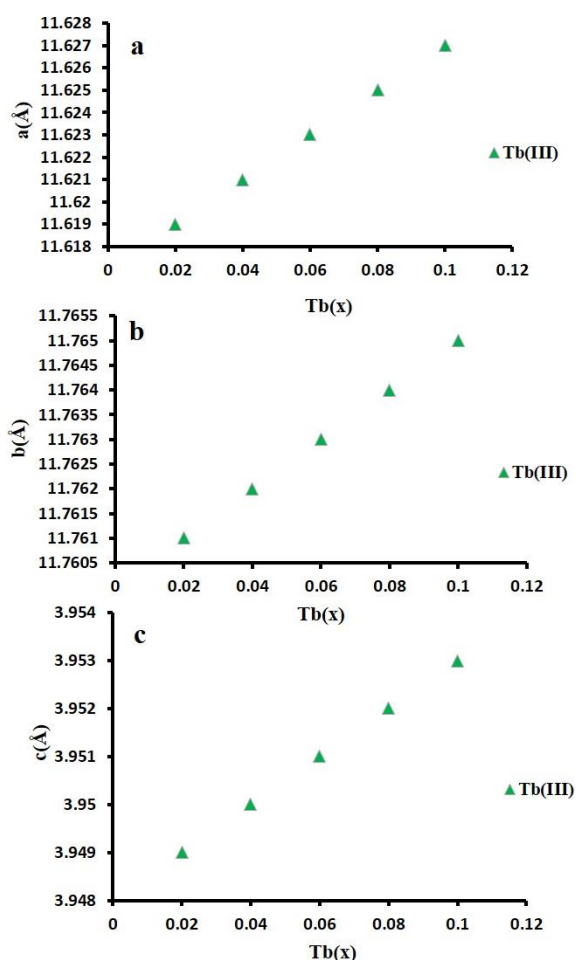


Figure 18. The a lattice constant (a) and b lattice constant (b) as well as c lattice constant (c) of  $Sb_{2-x}Tb_xSe_3$  ( $0 \leq x \leq 0.10$ ) dependent upon  $Tb^{3+}$ -doping on  $Sb^{3+}$  sites.

Figure 4 shows SEM images of  $Sb_2Se_3$  and  $Tb$ -doped  $Sb_2Se_3$ . Doping of  $Tb^{3+}$  into the structure of  $Sb_2Se_3$  changes the morphology from rods to particles. Figure 4a shows  $Sb_2Se_3$  nanorods with thicknesses of 70–200 nm. The diameter of  $Sb_{1.9}Tb_{0.1}Se_3$  particles is around 30 nm (Figure 4b).

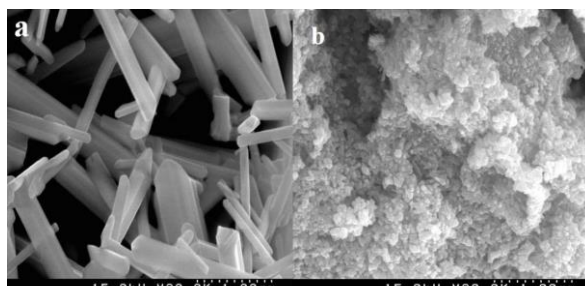


Figure 19. SEM image of  $Sb_2Se_3$  (a),  $Sb_{1.90}Tb_{0.1}Se_3$  nanoparticles (b) synthesized at  $160^\circ C$  and 24h.

The surface zone, normal pore measure, and normal pore volume of the  $Sb_{1.90}Tb_{0.1}Se_3$  nanoparticles were assessed. Earlier to  $N_2$ -physical adsorption estimations, the sample was degassed at  $150^\circ C$  for 120 min within the nitrogen environment. So, the particular surface range (SBET) of the gotten materials was decided with adsorption-desorption isotherms of  $N_2$  at 77 K. The information is summarized in Table 1. It can be seen that the normal surface zone and pore breadth are approximately  $1.84 \text{ m}^2 \text{ g}^{-1}$  and 20 nm.

Table 9. BET data for the fabricated samples.

Sample	BET surface area ( $\text{m}^2 \text{ g}^{-1}$ )	Pore diameter (nm)	Pore volume ( $\text{cm}^3 \text{ g}^{-1}$ )
$S_1$	1.84	20	0.0084

$Sb_2Se_3$  and its alloys are thermoelectric materials and have been investigated for direct conversion of thermal energy to electric energy as well as electronic refrigeration [30]. With the increase in the lanthanide concentration, the electrical resistivity of synthesized nanomaterials decreased obviously (Figure 5a). At room temperature, the electrical resistivity of pure  $Sb_2Se_3$  was of the order of  $0.2 \Omega \cdot \text{m}$  and in the case of  $Tb^{3+}$ -doped compounds the minimum value of electrical resistivity is  $0.03 \Omega \cdot \text{m}$ , respectively. The temperature dependence of the electrical resistivity for  $Tb$ -doped  $Sb_2Se_3$  between 290–350 K is shown in Figure 5b. Electrical resistivity decreases linearly with temperature. As a result, the electrical conductance of  $Tb$ -doped  $Sb_2Se_3$  materials is higher than pure  $Sb_2Se_3$  at room temperature and increases with temperature.

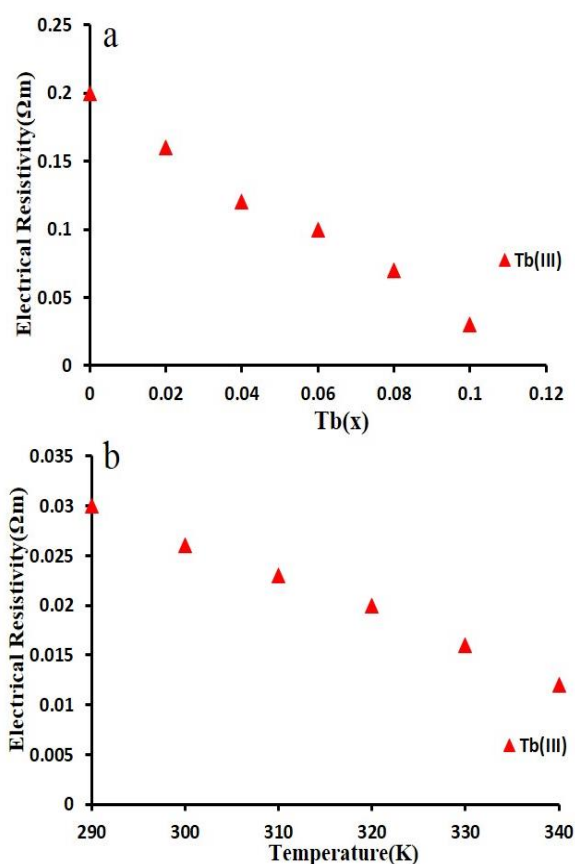


Figure 20. (a) Electrical resistivity and (b) thermoelectrical resistivity of  $Sb_{2-x}Tb_xSe_3$  nanoparticles.

### 3.2. Photocatalytic study

To explore the perfect conditions of photocatalytic performance, the degradation process of Rhodamine B (RB) was examined under visible light irradiation by  $Tb_xSb_{2-x}Se_3$  with various mole fractions ( $x = 0.00$  to  $x = 0.1$ ). Figure 6 demonstrates the degradation percent of Rhodamine B over divergent  $Tb^{3+}$ -doped  $Sb_2Se_3$  catalysts in 120 min of reaction. From Figure 6, it can be observed that the nanomaterials doped with proper content of  $Tb^{3+}$  ion had much enhanced photocatalytic performance than bare  $Sb_2Se_3$ , principally the sample with a 0.1 molar ratio of  $Tb^{3+}$ , which displayed the best catalytic activity. The reason for the high photocatalytic activity of  $Tb_{0.1}Sb_{1.90}Se_3$  can be described as follows: Normally, rare-earth cations can perform either as a recombination center or as a mediator of interfacial charge in the photocatalyst's crystalline structure [17, 18].

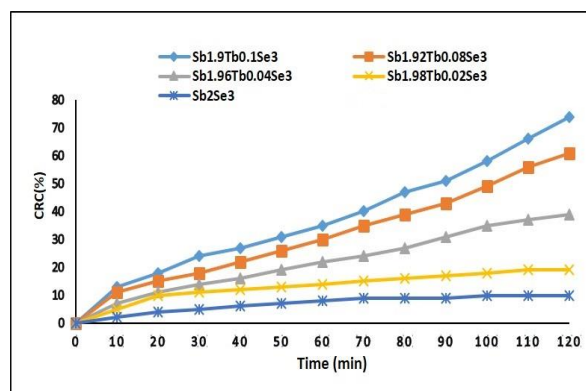


Figure 21. The effect of  $Tb^{3+}$  dopant content on the decolorization of 10 mg/L Rhodamine B (catalyst loading 1.0 g/L);

To properly explain the photocatalytic performance of the  $Tb_{0.1}Sb_{1.90}Se_3$  samples and assess the realizable mechanism of the reaction, the UV-Vis absorption spectra of RB at different irradiation times for the photocatalytic process are exhibited in Figure 7. The decreasing concentration of RB in the time of the catalytic procedure is utilized to evaluate the potential of the catalyst.

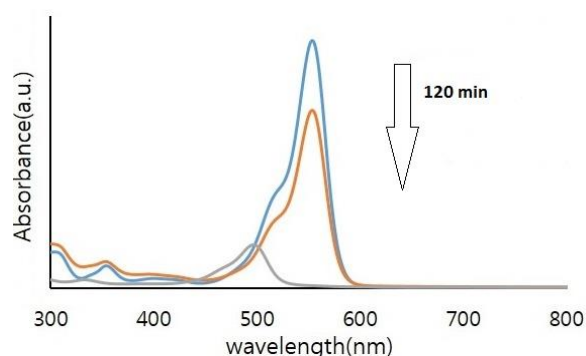
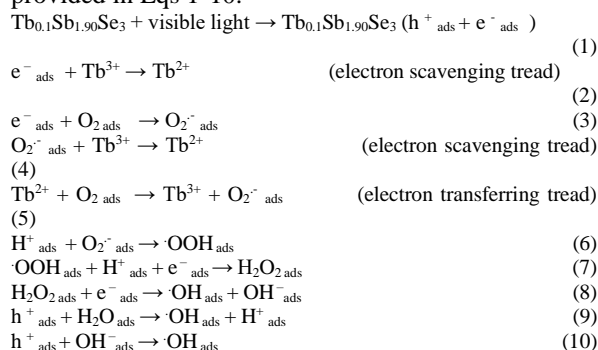


Figure 22. Adsorption and degradation of Rhodamine B under visible light irradiation using  $Tb_{0.1}Sb_{1.90}Se_3$  nanoparticles.

The decolorization mechanism for the  $Tb_{0.1}Sb_{1.90}Se_3$  is provided in Eqs 1-10.



The reusability is one of the most substantial parts of a catalyst. Figure 8 displays the reusability assays of  $Tb_{0.1}Sb_{1.90}Se_3$  catalyst in the degradation of Rhodamine B, during the 5 round tests under perfect conditions as 120 min for photocatalytic process, 10 mg/L of Rhodamine B, 1.0 g/L of  $Tb_{0.1}Sb_{1.90}Se_3$  photocatalyst.

Following each degradation test, the catalyst was washed with distilled water and then dried at 70 °C for 2h and so utilized in the next run. As shown in Figure 8,  $Tb_{0.1}Sb_{1.90}Se_3$  displayed outstanding chemical firmness without any significant decomposition or photo-corrosion during the 5 rounds of catalytic reaction which is an essential superior for empirical applications.

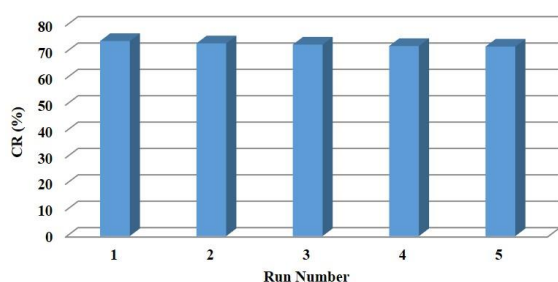


Figure 23. Reusability results of  $Tb_{0.1}Sb_{1.90}Se_3$  in photocatalytic decolorization of 10 mg/L of Rhodamine B and 120 min for irradiation time.

To study the decolorization process's mechanism and to explore the main oxidative species, assays were carried out in the presence of proper scavengers of active species. As shown in Figure 9, adding oxalate (a scavenger of  $h^+_{VB}$ ) results in the deduction of the decolorization percentage to 27.92%. In the case of benzoquinone (BQ) (a scavenger of superoxide radicals), the dye degradation was hindered extraordinarily. Adding t-BuOH (a scavenger of hydroxyl radicals) leads to a reduction of 47% in the decolorization percentage. Considering  $I^-$  (scavenger of the hole) it reaches 19.48 %, respectively. These results demonstrate that superoxide radicals and the  $h^+_{VB}$  were the principal oxidative species in decomposing dye structure. Nevertheless, the hydroxyl radicals also influence decolorization.

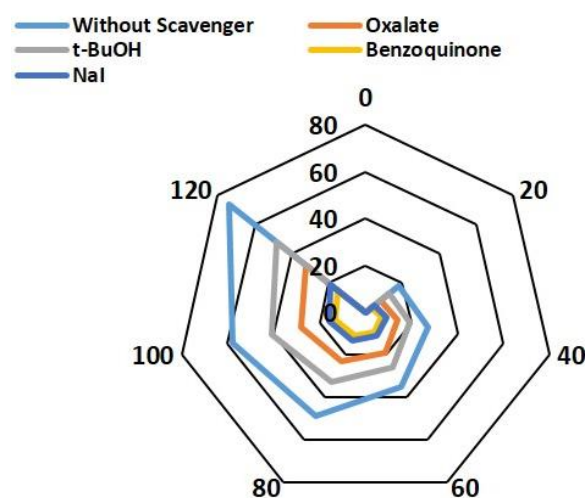


Figure 24. The effect of the addition of benzoquinone, butanol,  $I^-$  and oxalate ions on the decolorization of 10 mg/L RB ( $Tb_{0.1}Sb_{1.90}Se_3$  loading 1.0 g/L).

## Conclusion

In this research, pure and  $Tb^{3+}$ -doped  $Sb_2Se_3$  were prepared by a simple hydrothermal approach and were employed as photocatalysts under visible light irradiation for removal of Rhodamine B. XRD analysis displayed well crystalline cubic structure of  $Sb_2Se_3$ . The substitution of  $Tb^{3+}$  ions into the  $Sb_2Se_3$  lattice was validated by the EDS analysis. The surface morphology and size of the samples have obvious changes from rods to nanoparticles after incorporating  $Tb^{3+}$  into the lattice of  $Sb_2Se_3$ . Results indicated that the decolorization efficiency of  $Tb^{3+}$ -doped  $Sb_2Se_3$  was higher than pure  $Sb_2Se_3$ , and degradation efficiency was affected by the content of Tb dopant in  $Sb_2Se_3$ . The promoted decolorization efficiency was found in the presence of 10 %  $Tb^{3+}$ -doped  $Sb_2Se_3$  particles. The color removal percentage of  $Tb_{0.1}Sb_{1.90}Se_3$  and undoped  $Sb_2Se_3$  was 77.15 and 11.37% after 120 min of treatment, respectively. Benzoquinone caused the highest negative effect on the photocatalysis of Rhodamine B. Generally, the application of  $Tb^{3+}$ -doped  $Sb_2Se_3$  particles can be a promising and effective approach for the elimination of colored effluents.

## Acknowledgment

This work is funded by Sayyed Jamaledin Asadabadi University Research Grant.

## References

1. Khataee AR, Khataee A, Fathinia M, Hanifehpour Y, Joo SW. Kinetics and mechanism of enhanced photocatalytic activity under visible light using synthesized  $Px Cd_{1-x} Se$  nanoparticles. *Industrial Engineering Chemistry Research*. 2013; 52: 13357–13369.  
DOI: <https://doi.org/10.1021/ie402352g>
2. Hamnabard N, Hanifehpour Y, Khomami B, Joo SW. Synthesis, characterization and photocatalytic performance of Yb-doped CdTe nanoparticles. *Materials Letters*. 2015, 145: 253-257.  
DOI: <https://doi.org/10.1016/j.matlet.2015.01.074>
3. Tryk DA, Fujishima A, Honda K. Recent topics in photo electrochemistry: achievements and future prospects. *Electrochimica Acta*. 2000; 45: 2363-2376.  
DOI: [https://doi.org/10.1016/S0013-4686\(00\)00337-6](https://doi.org/10.1016/S0013-4686(00)00337-6)
4. S. Ahmed, M.G. Rasul, W.N. Martens, R. Brown, M.A. Hashib, Heterogeneous photocatalytic degradation of phenols in wastewater: A review on current status and developments, *Desalination*. 261 (2010) 3–18.  
DOI: <https://doi.org/10.1016/j.desal.2010.04.062>
5. Alemi A, Hanifehpour Y, Joo SW, Min BK. Synthesis of novel  $Ln_x Sb_{2-x} S_3$  (Ln:  $Lu^{3+}$ ,  $Ho^{3+}$ ,  $Nd^{3+}$ ) nanomaterials via co-reduction method and investigation of their physical properties. *Colloids and Surfaces A: Physicochemical Engineering Aspects*. 2011; 390: 142–148.  
DOI: <https://doi.org/10.1016/j.colsurfa.2011.09.018>
6. Hanifehpour Y, Joo SW. Synthesis, characterization and sonophotocatalytic degradation of an azo dye on

- Europium doped cadmium selenide nanoparticles. *Nanochemistry Research*.2018; 3(2): 178-188.  
DOI: <https://doi.org/10.22036/NCR.2018.02.007>
7. A. Khataee, S. Saadi, B. Vahid, S.W. Joo, B.-K. Min, Sonocatalytic degradation of Acid Blue 92 using sonochemically prepared samarium doped zinc oxide nanostructures, *Ultrason. Sonochem.* 29 (2016) 27–38.  
DOI: <https://doi.org/10.1016/j.ultsonch.2015.07.026>
8. C. Mastrovito, J.W. Lekse, J.A. Aitken, Rapid solid-state synthesis of binary group 15 chalcogenides using microwave irradiation. *J. Solid State Chem.* 180 (2007) 3262-3270.  
DOI: <https://doi.org/10.1016/j.jssc.2007.09.001>
9. X. Qiu, C. Burda, R. Fu, J. Zhu, et al., Heterostructured Bi<sub>2</sub>Se<sub>3</sub> Nanowires with Periodic Phase Boundaries. *J Am Chem Soc.* 126 (2004) 16276-16277.  
DOI: <https://doi.org/10.1021/ja045556r>
10. H. Ji, X. Zhao, Y. Zhang, B. Lu B ,H. Ni, Solvothermal synthesis and thermoelectric properties of lanthanum contained Bi–Te and Bi–Se–Te alloys .*Mater Lett.* 59 (2005) 682-685.  
DOI: <https://doi.org/10.1016/j.matlet.2004.11.008>
11. P. Janíček, C. Drasar, P. Losták , J. Vejpravová, Transport, magnetic, optical and thermodynamic properties of Bi<sub>2–x</sub>MnxSe<sub>3</sub> single crystals *Physica B.* 403(2008) 3553-3558.  
DOI: <https://doi.org/10.1016/j.physb.2008.05.025>
12. P. Lostak, C. Drasar, I. Klichova, T. Cernohorsky, Properties of Bi<sub>2</sub>Se<sub>3</sub> single crystals doped with Fe atoms *Phys Status Solidi B.* 200(1997) 289-296.  
DOI: [https://doi.org/10.1002/1521-3951\(199703\)200:1%3C289::AID-PSSB289%3E3.0.CO;2-8](https://doi.org/10.1002/1521-3951(199703)200:1%3C289::AID-PSSB289%3E3.0.CO;2-8)
13. S. Augustin, E. Mathai, Growth, morphology, and microindentation analysis of Bi<sub>2</sub>Se<sub>3</sub>, Bi<sub>1.8</sub>In<sub>0.2</sub>Se<sub>3</sub>, and Bi<sub>2</sub>Se<sub>2.8</sub>Te<sub>0.2</sub> single crystals. *Mater Res Bull.*36 (2001) 2251-2261.  
DOI: [https://doi.org/10.1016/S0025-5408\(01\)00717-6](https://doi.org/10.1016/S0025-5408(01)00717-6)
14. N.S. Patil, A.M. Sargar, S.R. Mane, P.N. Bhosale, Growth mechanism and characterization of chemically grown Sb doped Bi<sub>2</sub>Se<sub>3</sub> thin films *Appl Surf Sci.* 254(2007)5261-5265.  
DOI: <https://doi.org/10.1016/j.apsusc.2008.02.084>
15. P. Larson, R.L. Lambrecht, Electronic structure and magnetism in Bi<sub>2</sub>Te<sub>3</sub>, Bi<sub>2</sub>Se<sub>3</sub>, and Sb<sub>2</sub>Te<sub>3</sub> doped with transition metals (Ti–Zn) *Phys Rev B.* 78(2008) 195207-195214.  
DOI: <https://doi.org/10.1103/PhysRevB.78.195207>
16. X. Gratens, S. Isber, S. Charar, C. Fau, M. Averous, *Phys Rev B.* 55(1997) 8075-8078.  
DOI: <https://doi.org/10.1103/PhysRevB.55.8075>
17. Khataee AR, Hanifehpour Y, Safarpour M, Hosseini M, Joo SW. Synthesis and characterization of Er xZn1–x Se nanoparticles: a novel visible light responsive photocatalyst . *Science of Advanced Materials.* 2013; 5: 1074–1082.  
DOI: <https://doi.org/10.1166/sam.2013.1556>
18. Y. Hanifehpour, B. Soltani, A.R. Amani-Ghadim, B. Hedayati, B. Khomami, S.W. Joo, Synthesis and characterization of samarium-doped ZnS nanoparticles: A novel visible light responsive photocatalyst, *Mater. Res. Bull.* 76 (2016) 411–421.  
DOI: <https://doi.org/10.1016/j.materresbull.2015.12.035>